Peristaltic transport of a power-law fluid induced by a single wave: A numerical analysis using the cumulant lattice Boltzmann method

Maeyama, Kohei
Ishida, Shunichi
Imai, Yohsuke

(Citation)
Physics of Fluids,34(11):111911

(Issue Date)
2022-11-22

(Resource Type)
journal article

(Version)
Version of Record

Physics of Fluids

Peristaltic transport of a power-law fluid induced by a single wave: A numerical analysis using the cumulant lattice Boltzmann method

Cite as: Phys. Fluids **34**, 111911 (2022); https://doi.org/10.1063/5.0122182
Submitted: 22 August 2022 • Accepted: 02 November 2022 • Published Online: 22 November 2022

Kohei Maeyama (前山公平), **Shunichi Ishida** (石田駿一) and **Yohsuke Imai** (今井陽介)

Physics of Fluids ARTICLE scitation.org/journal/phf

Peristaltic transport of a power-law fluid induced by a single wave: A numerical analysis using the cumulant lattice Boltzmann method

Cite as: Phys. Fluids **34**, 111911 (2022); doi: 10.1063/5.0122182
Submitted: 22 August 2022 · Accepted: 2 November 2022 ·
Published Online: 22 November 2022

View Online Export Citation CrossMark

Kohei Maeyama (前山公平), Shunichi Ishida (石田駿一), and Yohsuke Imai (今井陽介)[a]

AFFILIATIONS

Graduate School of Engineering, Kobe University, Kobe 657-8501, Japan

[a]Author to whom correspondence should be addressed: yimai@mech.kobe-u.ac.jp. URL: https://www.lab.kobe-u.ac.jp/eng-afe/

ABSTRACT

Peristaltic pumping is the primary mechanism of food transport in the human intestine. Intestinal contents are often modeled as power-law fluids with low-behavior indices ($n < 1$). Peristaltic flows were studied for periodic contraction waves ($L/\lambda = 1$) with infinitely long wavelengths ($\lambda/D \to \infty$) in the Stokes flow regime ($Re \to 0$). However, the peristaltic flow generated by an isolated contraction wave with a short wavelength at nonzero Reynolds numbers is more relevant to physiological conditions. In this study, we investigated the peristaltic transport of a power-law fluid with a low behavior index of $n = 0.21$ at nonzero Reynolds numbers up to $Re = 10$, generated by a single short contraction wave. First, we investigated the analytical solution for the peristaltic transport of the power-law fluid for $\lambda/D \to \infty$ and $Re \to 0$. The analytical solution shows that the discharge flow rate of a power-law fluid generated by a single contraction wave is much smaller than that of a Newtonian fluid ($n = 1$). Next, we investigated the peristaltic transport for $Re \leq 10$ using the cumulant lattice Boltzmann method. The numerical results demonstrate that the discharge flow rate for the power-law fluid sharply increased owing to the inertia effect. The power-law fluid induces an asymmetric flow field with respect to the contraction wave at smaller Reynolds numbers than Newtonian fluids. The inertia effect was increased by the sharpness of the contraction wave. These results suggest that intestinal contents can be transported more quickly by an isolated contraction wave with a shorter wavelength when the contents have low consistency indices or when the contraction wave has a large propagation velocity.

I. INTRODUCTION

Peristaltic pumping is the mechanism of liquid transport generated by contraction waves along deformable channels. In the human intestine, chyme transformed from food is transported by peristaltic motions of the intestinal wall for digestion, absorption, and excretion. Peristaltic transport is also observed in other organs, such as the esophagus, stomach, and ureter. The most fundamental research on peristaltic flow is analytical solutions based on the lubrication theory. Shapiro *et al.*[1] derived an analytical solution for the peristaltic flow of Newtonian fluids for periodic contraction waves with infinitely long wavelengths at zero Reynolds numbers. Li and Brasseur[2] modified the classical lubrication theory model to investigate peristaltic flow generated by contraction waves with arbitrary wave numbers and channel lengths. Intestinal contents are often modeled as power-law fluids with low-behavior indices.[3] Shukla and Gupta[4] extended the theory of Shapiro *et al.*[1] to power-law fluids. They demonstrated that when the behavior index decreases, the amount of transported fluid decreased slightly. Power-law fluid flow through peristaltic channels with arbitrary axisymmetric shapes has also been investigated analytically. Srivastava and Srivastava[5] and Chaube *et al.*[6] investigated the peristaltic flow of power-law fluids through a nonuniform peristaltic channel. Misra and Pandey[7] studied the effect of single and train expansion waves on peristaltic transport of power-law fluids. Avvari[8] considered trade-off between the power consumption to propel power-law fluids and the local longitudinal shortening.

These analytical solutions are applicable to the Stokes flow regimes. However, if we assume that the diameter of the intestine is $D \sim 50$–75 mm,[9,10] the maximum peristaltic velocity is $C \sim 30$ mm/s,[9] density is $\rho \sim 10^3$ kg/m^3, consistency index is $k \sim 1$–3000 Pa s^n, the behavior index is $n \sim 0.21$,[3] and the Reynolds number reaches $Re \sim O(1)$ at most. Analytical solutions are also valid for infinitely long wavelengths, but some contraction waves have wavelengths similar to or shorter than the diameter of the intestine. Agbesi and Chevalier,[11] for example, reported short wavelengths of $\lambda/D \sim 0.5$–1.5 in the mice hindgut and chicken embryonic midgut.

In addition, the previous studies considered periodic waves, but contraction waves are often isolated in the intestine. Shikaya *et al.*[12] for example, visualized isolated contraction waves in the chicken embryonic gut. Thus, peristaltic flow generated by a single contraction wave with short wavelength at nonzero Reynolds number is more relevant to physiological conditions.

Recent studies have partly demonstrated the inertial effect on the peristaltic flow of power-law fluids.[13–15] Peristaltic transport by an isolated contraction wave has also been studied.[8,11,16] In addition, some studies focused on the dynamics of particles in peristaltic flows.[17–19] However, the peristaltic flow of power-law fluids with low-behavior indices is not fully understood. Motivated by the above, we investigate the peristaltic transport of a power-law fluid with a low-behavior index $n = 0.21$ at $Re \leq 10$, generated by a single contraction wave.

We present a computational framework for simulating the peristaltic flow of power-law fluids with low-behavior indices based on the lattice Boltzmann method (LBM).[20] The LBM does not directly solve the pressure and velocity fields and is efficient for parallel computing and complex wall boundaries. Furthermore, for power-law fluids, the shear rate is estimated locally using the LBM distribution function without finite differences. This benefit was first highlighted by Ginzburg.[21] However, the LBM for power-law fluids presents two difficulties in terms of numerical stability. First, the diffusion number (non-dimensional viscosity) can easily exceed the stable range in low-shear-rate regions. Second, the diffusion number (relaxation time) may be extremely small in high shear rate regions. Gabbanelli *et al.*[22] presented a truncated power-law model to limit the maximum and minimum viscosities. An improved LBM for power-law fluids was also developed in which additional forcing operators or reconstructed distribution functions were introduced.[23–25] Stabilized LBMs, such as multi-relaxation-time (MRT) LBM and cascaded LBM, have also been used for this problem.[26–28] The numerical conditions were also studied by Conrad *et al.*[29] However, the LBM for the peristaltic transport of power-law fluids has not yet been established. In this study, we propose a numerical method based on the cumulant LBM.[32]

The remainder of this paper is organized as follows: In Sec. II, we describe the problem statement and the numerical methods. In Sec. III, the analytical solution of the peristaltic flow is investigated for $\lambda/D \to \infty$ and $Re \to 0$, where λ/D denotes the wavelength relative to the channel diameter. In Sec. IV, we present the numerical results to clarify the effects of λ/D and Re on peristaltic flow. Finally, we discuss our results with a focus on physiological conditions in Sec. V.

II. NUMERICAL METHODS

A. Geometry

We consider the three-dimensional flow of power-law fluids driven by peristaltic contraction in a circular channel of length L and diameter D (Fig. 1). A contraction wave of wavelength λ propagates with contraction ratio D_p/D and wave speed C. The wave shape was determined by a sinusoidal function. The shape of the channel at position X and time t is expressed as follows:

$$H(X,t) = \begin{cases} D/2 - \dfrac{D_p}{4}\left\{1 + \cos\dfrac{2\pi}{\lambda}(X - Ct)\right\} & \left(-\dfrac{\lambda}{2} \leq X - Ct \leq \dfrac{\lambda}{2}\right), \\ D/2 & (\text{otherwise}). \end{cases} \tag{1}$$

In this paper, the position and velocity vectors in the laboratory frame are denoted by $\boldsymbol{X} = (X, Y, Z)$ and $\boldsymbol{U} = (U, V, W)$, and those in the moving frame are $\boldsymbol{x} = (x, y, z)$ and $\boldsymbol{u} = (u, v, w)$. These parameters are transformed by the following equations:

$$x = X - Ct, \quad y = Y, \quad z = Z, \tag{2}$$

$$u = U - C, \quad v = V, \quad w = W. \tag{3}$$

The shape of the channel in the moving frame is expressed as follows:

$$h(x) = \begin{cases} D/2 - \dfrac{D_p}{4}\left(1 + \cos\dfrac{2\pi}{\lambda}x\right) & \left(-\dfrac{\lambda}{2} \leq x \leq \dfrac{\lambda}{2}\right), \\ D/2 & (\text{otherwise}). \end{cases} \tag{4}$$

Physical quantities are summarized in Table I.

B. Governing equations

The governing equations are the Navier–Stokes and continuity equations for incompressible fluids as follows:

$$\rho\left(\frac{\partial \boldsymbol{U}}{\partial t} + \boldsymbol{U}\cdot\nabla\boldsymbol{U}\right) = \nabla\cdot\boldsymbol{\sigma}, \tag{5}$$

$$\nabla\cdot\boldsymbol{U} = 0, \tag{6}$$

where ρ denotes the fluid density and $\boldsymbol{\sigma}$ denotes the stress tensor. The stress tensor is obtained as follows:

$$\boldsymbol{\sigma} = -p\boldsymbol{I} + 2\mu\boldsymbol{E}, \tag{7}$$

where p denotes the pressure, μ denotes the apparent viscosity, and $\boldsymbol{E}$ denotes the rate of strain tensor. The rate of strain tensor is obtained from the velocity gradients as follows:

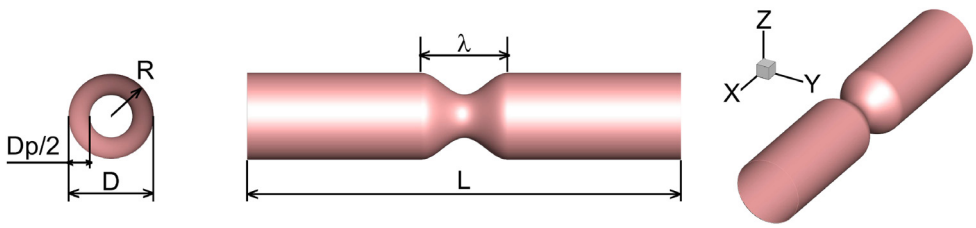

FIG. 1. Wall geometry of the peristalsis. D denotes the channel diameter, $R = D/2$ denotes the channel radius, and L denotes the channel length. D_p denotes the amplitude of the contraction wave, and λ denotes the wavelength.

TABLE I. Physical quantities.

Symbols	Quantities
D	Channel diameter
L	Channel length
λ	Wavelength
D_p	Contraction amplitude
C	Wave velocity
$\boldsymbol{U}$	Velocity vector in the laboratory frame
$\boldsymbol{u}$	Velocity vector in the moving frame
$\lvert\dot{\gamma}\rvert$	Shear rate
Re	Reynolds number
p	Pressure
Q	Discharge flow rate

$$E_{ij} = \frac{1}{2}\left(\frac{\partial U_i}{\partial X_j} + \frac{\partial U_j}{\partial X_i}\right). \tag{8}$$

The apparent viscosity of power-law fluids is expressed as follows:[31]

$$\mu(|\dot{\gamma}|) = k|\dot{\gamma}|^{n-1}, \tag{9}$$

where the constants k and n are known as the consistency index and the behavior index, respectively, and $\dot{\gamma}$ denotes the shear rate obtained as follows:

$$|\dot{\gamma}| = \sqrt{2E_{ij}E_{ij}}. \tag{10}$$

The governing equations are solved in the moving frame, with no-slip boundary conditions at the wall, and zero-pressure boundary conditions at both the ends of the channel. We define the Reynolds number as follows:

$$\begin{aligned} Re &= \frac{\rho CD}{\mu(C/D)} \\ &= \frac{\rho CD}{k(C/D)^{n-1}} \\ &= \frac{\rho C^{2-n}D^n}{k}. \end{aligned} \tag{11}$$

C. Lattice Boltzmann method

We simulated the peristaltic transport of power-law fluids using LBM,[20] as in our previous study on the peristaltic transport of Newtonian fluids.[16] The time evolution equation of the distribution function $f_{\xi\eta\zeta}$ for the lattice direction $\xi, \eta, \zeta \in \{-1, 0, 1\}$ reads

$$f^*_{\xi\eta\zeta}(\boldsymbol{x}, t) = f_{\xi\eta\zeta}(\boldsymbol{x}, t) + \Omega_{\xi\eta\zeta}, \tag{12}$$

$$f_{\xi\eta\zeta}(\boldsymbol{x} + \boldsymbol{c}_{\xi\eta\zeta}\Delta t, t + \Delta t) = f^*_{\xi\eta\zeta}(\boldsymbol{x}, t), \tag{13}$$

where $\boldsymbol{x}$ denotes the position, t denotes time, $\boldsymbol{c}_{\xi\eta\zeta}$ denotes the particle velocity, and $\Omega_{\xi\eta\zeta}$ denotes the collision operator.

In the case of power-law fluids with a low behavior index ($n < 1$), the apparent viscosity locally decreases in high shear rate regions, possibly resulting in numerical instabilities. Here, we use the D3Q27 cumulant model[32] as a stabilization technique for numerical simulations of power-law fluids. In the cumulant LBM, the collision of particles is modeled in a cumulant space. The cumulant $C_{\alpha\beta\gamma}$ for $f_{\xi\eta\zeta}$ is defined as

$$C_{\alpha\beta\gamma} = c^{-\alpha-\beta-\gamma}\frac{\partial^\alpha\partial^\beta\partial^\gamma}{\partial\Xi^\alpha\partial\Upsilon^\beta\partial Z^\gamma}\ln\left(F(\boldsymbol{\Xi})\right)|_{\Xi=\Upsilon=Z=0}, \tag{14}$$

where $\boldsymbol{\Xi} = (\Xi, \Upsilon, Z)$ is the momentum wave number, $\alpha, \beta, \gamma, \in \{0, 1, 2\}$ are the indices of the cumulant, and $F(\boldsymbol{\Xi})$ is the Laplace-transformed distribution function. The collision of cumulant is described by the following equation:

$$C^*_{\alpha\beta\gamma} = (1 - \omega_{\alpha\beta\gamma})C_{\alpha\beta\gamma} + \omega_{\alpha\beta\gamma}C^{\mathrm{eq}}_{\alpha\beta\gamma}, \tag{15}$$

where C^* is the post-collision cumulant, C^{eq} is the equilibrium value of cumulant, and $\omega_{\alpha\beta\gamma}$ is the relaxation rate for cumulant LBM. The second-order cumulants relate to shear viscosity; $\omega_{200} = \omega_{020} = \omega_{002} = \omega_{110} = \omega_{101} = \omega_{011} = \omega_1 = 1/\tau$ and they have leading influence on numerical results. The other relaxation rate can be selected arbitrary from a range of 0–2. In this study, we set the other relaxation parameter to 1. The post collision distribution function $f^*_{\xi\eta\zeta}$ is calculated by the Laplace inverse transformation of cumulant $C^*_{\xi\eta\zeta}$.

In conventional numerical methods, the rate of strain tensor can be computed by finite-difference approximation using velocity data on neighboring nodes. However, in the cumulant LBM, the rate of strain tensor is locally discretized using the summation of the cumulant without adjacent information.[30] Then, the shear rate norm was approximated as follows:

$$|\dot{\gamma}| \approx \sqrt{2E^{\mathrm{d}}_{ij}E^{\mathrm{d}}_{ij}} + \varepsilon, \tag{16}$$

where

$$\begin{aligned} E^{\mathrm{d}}_{11} = &-\frac{\omega_1}{2\rho}(2C_{200} - C_{020} - C_{002}) \\ &-\frac{1}{2\rho}(C_{200} + C_{020} + C_{002} - \kappa_{000}), \end{aligned} \tag{17}$$

$$E^{\mathrm{d}}_{22} = E^{\mathrm{d}}_{11} + \frac{3\omega_1}{2\rho}(C_{200} - C_{020}), \tag{18}$$

$$E^{\mathrm{d}}_{33} = E^{\mathrm{d}}_{11} + \frac{3\omega_1}{2\rho}(C_{200} - C_{002}), \tag{19}$$

$$E^{\mathrm{d}}_{12} = -\frac{3\omega_1}{2\rho}C_{110}, \tag{20}$$

$$E^{\mathrm{d}}_{23} = -\frac{3\omega_1}{2\rho}C_{011}, \tag{21}$$

$$E^{\mathrm{d}}_{31} = -\frac{3\omega_1}{2\rho}C_{101}, \tag{22}$$

and ε denotes the artificial shear rate (ASR). The notation κ_{000} denotes the central moment for $\alpha = \beta = \gamma = 0$. ASR was added to prevent the apparent viscosity from approaching infinity in low-shear-rate regions.

For curved moving wall boundary conditions, interpolated-bounce-back scheme[33] is used.

In the LBM, the collision step is characterized by the relaxation time τ. This is a non-dimensional parameter defined as follows:

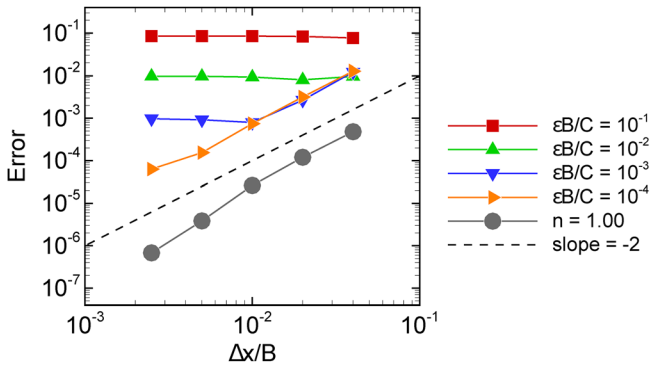

FIG. 2. Effect of ASR on the numerical solution of 2D Poiseuille flow for $n = 0.21$, where ε denotes the ASR, B denotes the parallel wall distance, C denotes the wave velocity, and Δx denotes the lattice spacing. The referential diffusion number is $Df_{\mathrm{ref}} = 0.1$. The results of a Newtonian fluid ($n = 1$) are also provided. The dashed line indicates second-order convergence.

$$\tau = \frac{1}{2} + 3Df, \tag{23}$$

where Df denotes the diffusion number

$$Df = \frac{\mu \Delta t}{\rho \Delta x^2}. \tag{24}$$

For power-law fluids, the diffusion number varies with the local shear rate. Thus, we introduce a reference diffusion number Df_{ref} as follows:

$$Df_{\mathrm{ref}} = \frac{k\Delta t}{\rho \Delta x^2} |\dot{\gamma}|_{\mathrm{mean}}^{n-1}. \tag{25}$$

Here, $|\dot{\gamma}|_{\mathrm{mean}}$ denotes the mean shear rate, and we estimate it as $|\dot{\gamma}|_{\mathrm{mean}} = C/D$ to characterize the global viscosity in the computation domain.

The influence of the ASR on the numerical solution of a two-dimensional (2D) Poiseuille flow (see Appendix A) is shown in Fig. 2, where the distance between the parallel plates is denoted by B. The cumulant LBM has a second-order accuracy with respect to the grid size for Newtonian fluids ($n = 1$). When ASR is set as $\varepsilon B/C = 10^{-4}$, the proposed method also has second-order accuracy for the power-law fluid with $n = 0.21$, at least for a range from $\Delta x/B = 1/25$ to $\Delta x/B = 1/400$. Second-order schemes have also been presented in the previous studies.[23–29,34] Hereinafter, we use $\varepsilon B/C = 10^{-4}$ ($\varepsilon D/C = 10^{-4}$ for peristaltic transport) unless otherwise noted.

III. ANALYTICAL SOLUTIONS

First, we investigated the analytical solution of the peristaltic flow generated by a single contraction wave for $\lambda/D \to \infty$ and $Re \to 0$. The analytical solution was obtained using the lubrication theory.[1,2,4] For a three-dimensional channel, the relationship between the pressure gradient and flow rate is as follows:

$$\frac{dp}{dx} = -2k\left(\frac{3n+1}{\pi n}\right)^n \frac{1}{h^{3n+1}}(q + \pi Ch^2)|q + \pi Ch^2|^{n-1}, \tag{26}$$

where the flow rate is as follows:

$$q = \int_0^h 2\pi u r dr, \tag{27}$$

and the derivation of the analytical solution is presented in Appendix B. The flow rate in the laboratory frame is defined as follows:

$$Q = \int_0^h 2\pi(u + C) r dr = q + \pi Ch^2, \tag{28}$$

called discharge flow rate. In this study, the discharge flow rate at the outlet ($X = L$) was calculated.

The contraction ratio may vary over a wide range in physiological conditions. Agbesi and Chevalier,[11] for example, observed $D_p/D \sim 0.12$–0.88 in their animal experiments. Figure 3(a) shows the change in the discharge flow rate with the contraction ratio, where $L/\lambda = 5$. The discharge flow rate gradually increases with the contraction ratio for $n = 1$. In the case of $n = 0.21$, however, the discharge flow rate does not increase with the contraction ratio for the low and middle values of D_p/D but steeply increases for large values ($D_p/D \sim 0.75$ or larger).

Figure 3(b) compares the discharge flow rate between $n = 1$ and $n = 0.21$ as a function of L/λ. When L/λ is larger, the discharge flow rate decreases for $n = 1$ and $n = 0.21$, but the discharge flow rate for $n = 0.21$ more quickly decays. This results in a large difference in the discharge flow rate between Newtonian and power-law fluids for a single contraction wave. The discharge flow rate for power-law fluids highly depends on the channel length relative to the wavelength.

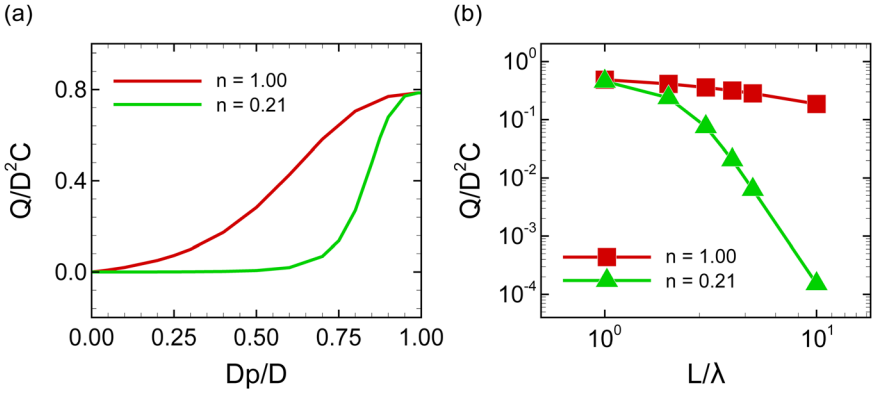

FIG. 3. Analytical solutions of discharge flow rate for $Re \to 0$ and $\lambda/D \to \infty$ (a) as a function of contraction ratio D_p/D for $L/\lambda = 5$ and (b) as a function of L/λ for $D_p/D = 0.5$.

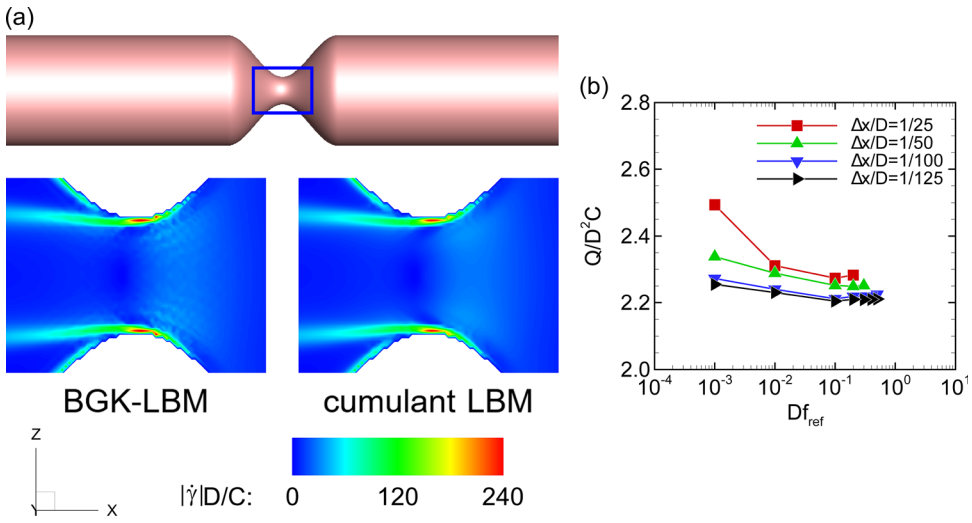

FIG. 4. Validation of the present method for peristaltic flow of a power-law fluid with $n = 0.21$, where $Re = 10$, $D_p/D = 0.75$, $L/\lambda = 5$, and $\lambda/D = 1$. (a) Nonphysical oscillations appear at the contracted region of the channel in BGK-LBM, whereas such oscillations do not appear in the cumulant LBM. (b) Effect of the lattice spacing and referential diffusion number on discharge flow rate.

IV. NUMERICAL RESULTS

In the present problem, four parameters were expected to influence the flow characteristics: D_p/D, L/λ, λ/D, and Re. The effects of D_p/D and L/λ are discussed in Sec. III, using analytical solutions. In this section, numerical simulation are used to examine the effect of λ/D and Re.

A. Validation

We first investigated whether the cumulant LBM can suppress the numerical instability that occurs in power-law fluid simulations. We compared the numerical results between the Bhatnagar–Gross–Krook LBM (BGK-LBM) and cumulant LBM for $D_p/D = 0.75$, $Re = 10$, $\lambda/D = 1$, and $L/\lambda = 5$ in Fig. 4(a). In BGK-LBM, nonphysical oscillations appear in the contracted region of the channel. The shear rate increases in this region, and the apparent viscosity decreases according to the power law. This cause Df to be small, resulting in a numerical instability. However, such oscillations were not observed in the cumulant LBM. These results suggest that a cumulant LBM can be used to avoid the numerical instability problem of power-law fluids.

We also test the convergence of the numerical solution with respect to $\Delta x/D$ and Df_{ref}. Figure 4(b) shows the effect of $\Delta x/D$ and Df_{ref} on the discharge flow rate. The numerical results were almost the same for $\Delta x/D = 1/100$ and $\Delta x/D = 1/125$ for $0.1 \le Df_{\mathrm{ref}} \le 0.5$. Therefore, in Secs. IV B–IV D and V and Appendix C, $\Delta x/D = 1/125$ and $Df_{\mathrm{ref}} = 0.1$ are used.

B. Effects of λ/D

Next, we investigated the effects of λ/D at a low Reynolds number of $Re = 0.1$. Figures 5(a) and 5(b) show the discharge flow rates for $n = 1$ and $n = 0.21$ as a function of λ/D, where $D_p/D = 0.5$ and $L/\lambda = 1$. Newtonian and power-law fluids exhibit nearly the same dependence on λ/D. The effect of λ/D on the discharge flow rate is limited to short wavelengths of approximately $\lambda/D \sim 1$. When λ/D increases, the discharge flow rate converges to that obtained from the analytical solution for $\lambda/D \to \infty$.

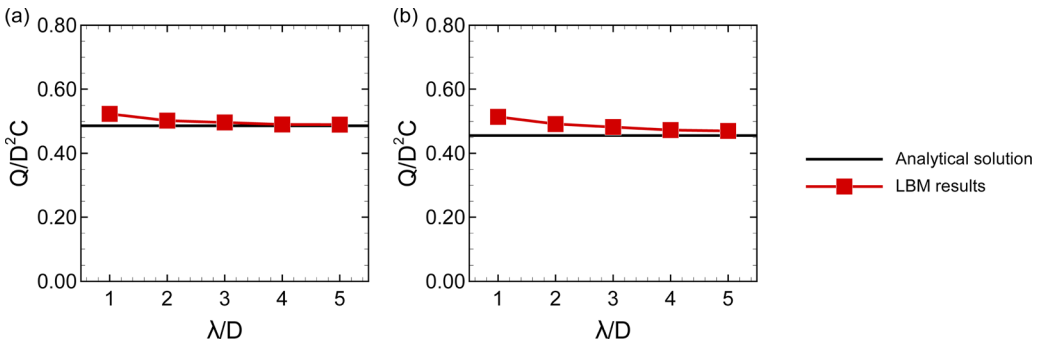

FIG. 5. Discharge flow rate as a function of λ/D for $Re = 0.1$, $D_p/D = 0.5$, and $L/\lambda = 1$: (a) $n = 1$ and (b) $n = 0.21$.

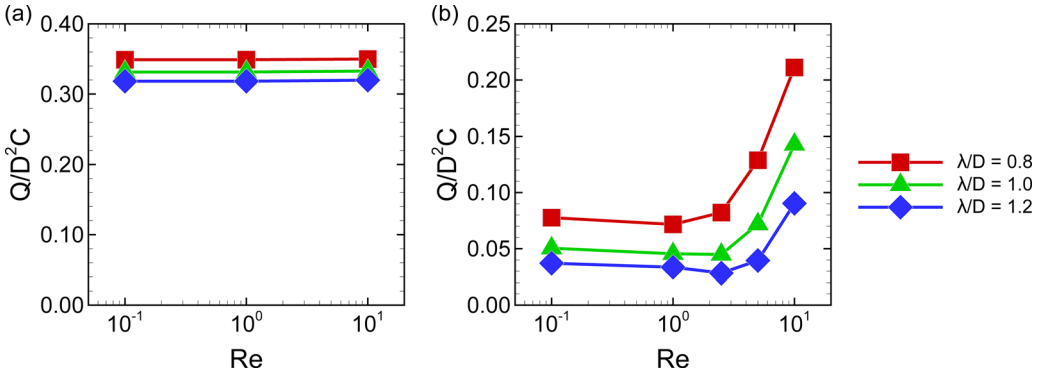

FIG. 6. Discharge flow rate as a function of *Re*, where $L/\lambda = 5$ and $D_p/D = 0.5$: (a) $n = 1$ and (b) $n = 0.21$.

C. Effects of *Re*

Subsequently, we investigated the effect of *Re* on the peristaltic flow of a power-law fluid. In Fig. 6, the discharge flow rate is shown as a function of *Re* for $D_p/D = 0.5$ and $L/\lambda = 5$, where λ/D varies from 0.8 to 1.2 (approximately 1). For $n = 1$, there was little change in the discharge flow rate, even when *Re* increased to 10. In contrast, the discharge flow rate increases sharply for $n = 0.21$. In addition, the discharge flow rate began to increase at a lower *Re* value when λ/D decreased. This indicates that the peristaltic transport of power-law fluids induced by a single contraction wave is highly dependent on *Re* and λ/D.

D. Velocity field and pressure

To find the mechanism of changes in the discharge flow rate with *Re*, we studied the velocity and pressure fields generated by a single contraction wave. We compare streamlines on the laboratory frame between $Re = 0.1$ and $Re = 10$ in Fig. 7, where $L/\lambda = 5$, $\lambda/D = 1$, and $D_p/D = 0.5$. In the case of $n = 1$, the velocity fields were almost the same for $Re = 0.1$ and 10. In contrast, the case of $n = 0.21$, an asymmetric velocity field appears with respect to the contraction wave for $Re = 10$, with stronger retrograde flow than the other cases.

The analytical solution suggests that the flow rate is proportional to $(dp/dx)^{1/n}$ for power-law fluids because of apparent viscosity (see Appendix B). The cross-sectional mean pressure is presented for $L/\lambda = 5$, $L/D = 1$, and $D_p/D = 0.5$ in Fig. 8, where the numbers with arrows indicate the slope of the least squares fit in the straight region of the channel. For $n = 0.21$, because of the strong retrograde flow, the pressure drop occurring in the contracted region is much larger for $Re = 10$ than for $Re = 0.1$ and increases the magnitude of the pressure gradient in the straight region of the channel. In Fig. 8(b), the pressure gradient for $Re = 10$ becomes approximately 1.3 times larger than that for $Re = 0.1$, and this pressure gradient may cause three times larger flow rate in Fig. 6(b).

V. DISCUSSION

First, we considered the analytical solution of this problem for $\lambda/D \to \infty$ and $Re \to 0$. The discharge flow rate of the power-law fluid is much smaller than that of Newtonian fluids. Shukla and Gupta[4] compared the peristaltic flows generated by periodic contraction waves ($L/\lambda = 1$) between Newtonian and power-law fluids. They reported that the flow rates were almost identical. The discrepancy between their results and ours is likely caused by the difference between the isolated and periodic waves, in particular, by the effect of L/λ on the discharge flow rate. As shown in Fig. 3(b), although the discharge flow rates are nearly the same for $n = 1$ and $n = 0.21$ at

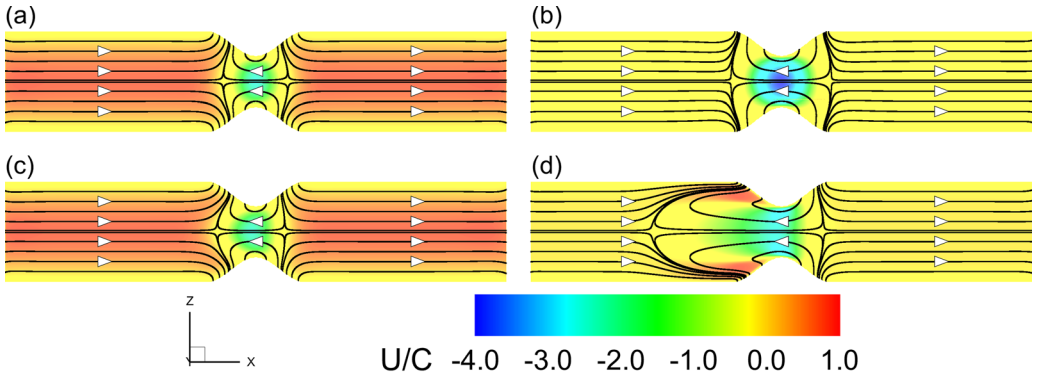

FIG. 7. Laboratory frame streamlines with x-directional velocity magnitude *U*/*C* at the center plane (XZ plane) of the channel, where $L/\lambda = 5$, $\lambda/D = 1$, and $D_p/D = 0.5$: (a) $Re = 0.1$ and $n = 1$; (b) $Re = 0.1$ and $n = 0.21$; (c) $Re = 10$ and $n = 1$; and (d) $Re = 10$ and $n = 0.21$.

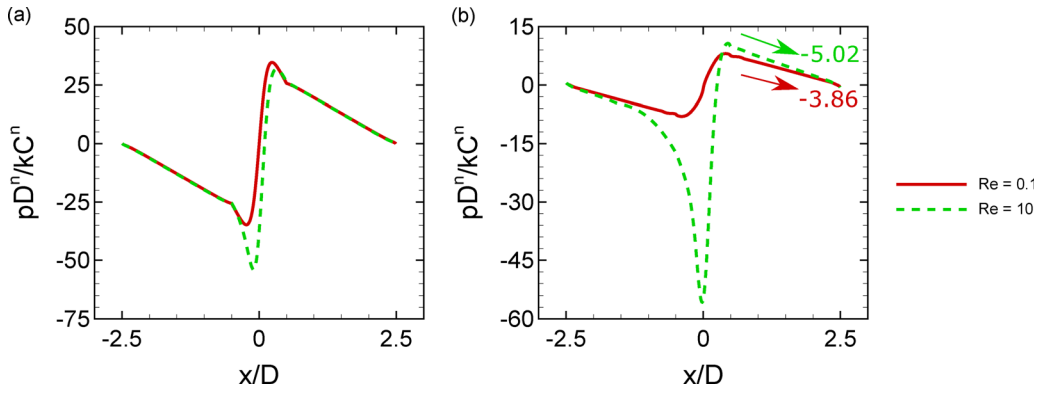

FIG. 8. Cross-sectional mean pressure along the channel for $L/\lambda = 5$, $\lambda/D = 1$, and $D_p/D = 0.5$: (a) $n = 1$ and (b) $n = 0.21$. The numbers with arrows indicate the slope of the least squares fit at the straight region of the channel.

$L/\lambda \sim 1$, the discharge flow rate of $n = 0.21$ is much smaller than that of $n = 1$ at a large value of L/λ.

Next, we performed numerical simulations to investigate the peristaltic flow of the power-law fluid at nonzero Reynolds numbers up to $Re = 10$. We present a computational framework for power-law fluids based on a cumulant LBM with an ASR. The numerical results demonstrate that the discharge flow rate for the power-law fluid with $n = 0.21$ sharply increased even at $Re = 10$, owing to the inertia effect. When a power-law fluid is transported by a single contraction wave with a short wavelength, an asymmetric flow field appears with respect to the contraction wave at $Re = 10$. Such an asymmetric velocity profile is not an inherent property of peristaltic flow of power-law fluids. As demonstrated in a previous study,[16] an asymmetric velocity profile appears at $Re = 100$ for Newtonian fluids. These results indicate that power-law fluids with low behavior indices tend to generate asymmetric flows, even at lower Reynolds numbers, than Newtonian fluids.

The inertia effect was increased by the sharpness of the contraction wave, or λ/D. In Fig. 6, we changed the channel length relative to the channel diameter, L/D, but the discharge flow rate at a fixed L/D may be more useful under physiological conditions. Figure 9 shows the discharge flow rate at $L/D = 5$ as a function of Re, where $D_p/D = 0.5$. At a low Re, the discharge flow rate is higher for larger values of λ/D; this relationship is inverted at $Re \sim 10$. This suggests that the intestinal contents can be transported more quickly by an isolated contraction wave with a shorter wavelength when Re is increased. In the human intestine, the Reynolds number may reach $Re \sim O(1)$ for intestinal contents with low consistency indices or fast propagation of contraction waves under pathological conditions. For example, in patients with irritable bowel syndrome, in which diarrhea is the predominant symptom, intestinal contents are transported more rapidly.[35,36] This may be associated with an increase in the Reynolds number and a decrease in the wavelength. Our results would be helpful for understanding intestinal transport in such patients.

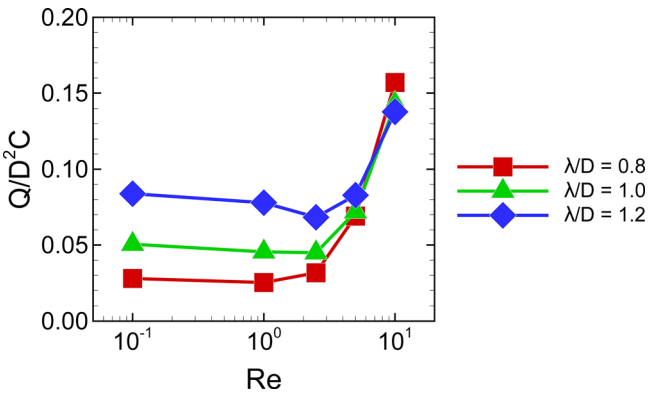

FIG. 9. Discharge flow rate as a function of Re, where $L/D = 5$, $D_p/D = 0.5$, and $n = 0.21$.

VI. CONCLUSIONS

We have presented the peristaltic transport of a power-law fluid with a low behavior index of $n = 0.21$, induced by a single contraction wave. The discharge flow rate for the power-law fluid sharply increased owing to the inertia effect. The power-law fluid induces an asymmetric flow field with respect to the contraction wave at smaller Reynolds numbers than Newtonian fluids. The results suggest that intestinal contents can be transported more quickly when the contents have low-consistency indices or when the contraction wave has a large propagation velocity.

ACKNOWLEDGMENTS

We thank Dr. H. Takeda and Mr. T. Oyama for helpful discussions. This work was supported by the Japan Society for the Promotion of Science (JSPS) KAKENHI Grant Nos. 19K20672 and 21H05785.

AUTHOR DECLARATIONS

Conflict of Interest

The authors have no conflicts to disclose.

Author Contributions

Kohei Maeyama: Data curation (lead); Formal analysis (lead); Investigation (lead); Methodology (equal); Software (equal); Validation (lead); Visualization (lead); Writing – original draft (lead); Writing – review & editing (equal). **Shunichi Ishida:** Data curation (supporting);

Formal analysis (supporting); Investigation (supporting); Methodology (equal); Resources (equal); Software (lead); Validation (supporting); Visualization (supporting); Writing – review & editing (supporting). **Yohsuke Imai:** Conceptualization (lead); Funding acquisition (lead); Investigation (supporting); Methodology (equal); Project administration (lead); Resources (lead); Supervision (lead); Writing – original draft (supporting); Writing – review & editing (lead).

DATA AVAILABILITY

The data that support the findings of this study are available from the corresponding author upon reasonable request.

APPENDIX A: ANALYTICAL SOLUTION OF 2D POISEUILLE FLOW

The analytical solution of the 2D Poiseuille flow for power-law fluids is obtained as follows:

$$u = \frac{n}{n+1}\left(\frac{1}{k}\frac{dp}{dx}\right)^{\frac{1}{n}}\left\{\left(\frac{B}{2}\right)^{1+\frac{1}{n}} - |y|^{1+\frac{1}{n}}\right\}, \tag{A1}$$

where x and y are the components of the position vector, u denotes the x-directional velocity, p denotes the pressure, B denotes the distance between parallel plates, and k and n denote the consistency and behavior indices, respectively. In Fig. 2, the numerical error is defined as follows:

$$Error = \sqrt{\frac{1}{N}\sum_{node}^{N}\left(\frac{u_{\mathrm{LBM},node} - u_{\mathrm{th},node}}{u_{\mathrm{th},node}}\right)^2}, \tag{A2}$$

where $u_{\mathrm{LBM},node}$ and $u_{\mathrm{th},node}$ ($\neq 0$) denote the numerical and analytical solutions at computational node, respectively, and N denotes the number of computational nodes.

APPENDIX B: ANALYTICAL SOLUTION OF 3D PERISTALTIC FLOW

Using the lubrication theory, the cylindrical form of Eq. (5) can be simplified as follows:

$$\frac{dp}{dx} = \mathrm{sgn}\left(\frac{\partial u}{\partial r}\right)\frac{k}{r}\frac{\partial}{\partial r}\left(r\left|\frac{\partial u}{\partial r}\right|^n\right), \tag{B1}$$

where r and u denote the radial position and axial velocity, respectively. Using the following boundary conditions:

$$\frac{\partial u}{\partial r} = 0 \ \text{at} \ r = 0, \quad u = -C \ \text{at} \ r = h \tag{B2}$$

we obtain the Poiseuille-type velocity profile as follows:

$$u = -C - \mathrm{sgn}\left(\frac{dp}{dx}\right)\left|\frac{1}{2k}\frac{dp}{dx}\right|^{\frac{1}{n}}\frac{n}{n+1}\left(h^{1+\frac{1}{n}} - r^{1+\frac{1}{n}}\right). \tag{B3}$$

Then, the flow rate is expressed as follows:

$$\begin{aligned} q &= \int_0^{h(x)} 2\pi r u dr, \\ &= -\pi C h^2 - \pi \mathrm{sgn}\left(\frac{dp}{dx}\right)\left|\frac{1}{2k}\frac{dp}{dx}\right|^{\frac{1}{n}}\frac{n}{3n+1}h^{3+\frac{1}{n}} \end{aligned} \tag{B4}$$

and we obtain the following:

$$\frac{dp}{dx} = -2k\left(\frac{3n+1}{\pi n}\right)^n \frac{1}{h^{3n+1}}\left(q + \pi C h^2\right)\left|q + \pi C h^2\right|^{n-1}. \tag{B5}$$

APPENDIX C: D3Q27 MRT-LBM

We also tested D3Q27 multiple-relaxation-time (MRT) LBM. In this paper, we follow Geier *et al.*[32] The moment $M_{\alpha\beta\gamma}$ is given by

$$M_{\alpha\beta\gamma} = c^{-\alpha-\beta-\gamma}\frac{\partial^\alpha\partial^\beta\partial^\gamma}{\partial\Xi^\alpha\partial\Upsilon^\beta\partial Z^\gamma}F(\Xi)|_{\Xi=\Upsilon=Z=0}. \tag{C1}$$

The collision of the particles is written as

$$M^*_{\alpha\beta\gamma} = (1 - s_{\alpha\beta\gamma})M_{\alpha\beta\gamma} + s_{\alpha\beta\gamma}M^{\mathrm{eq}}_{\alpha\beta\gamma}, \tag{C2}$$

where $M^*_{\alpha\beta\gamma}$ denotes the post-collision moment, $M^{\mathrm{eq}}_{\alpha\beta\gamma}$ denotes the moment for equilibrium, and $s_{\alpha\beta\gamma}$ denotes the relaxation parameter for MRT-LBM. In this paper, we set the relaxation parameter as

$$\begin{aligned} s_{\alpha\beta\gamma} = \{&0, 0, 0, 0, 0.8, \omega_1, \omega_1, \omega_1, \omega_1, \omega_1, \\ &0.8, 0.8, 0.8, 0.8, 0.8, 0.8, 0.8, 0.8, \\ &\omega_1, \omega_1, \omega_1, \omega_1, \omega_1, 0.8, 0.8, 0.8, \omega_1\}. \end{aligned} \tag{C3}$$

We simulated the same problems as Fig. 4 using MRT-LBM. The MRT-LBM can be applied to this problem, but a slight oscillation near the contraction appears (Fig. 10). The relaxation parameter must be optimized to obtain more proper result.

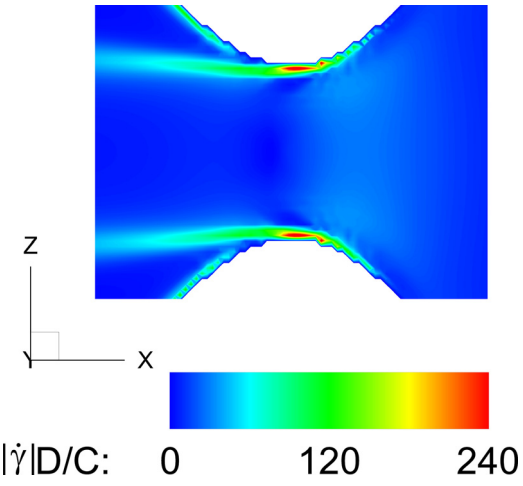

FIG. 10. Numerical result of MRT-LBM for the same problem as Fig. 4.

REFERENCES

[1]A. H. Shapiro, M. Y. Jaffrin, and S. L. Weinberg, "Peristaltic pumping with long wavelengths at low Reynolds number," J. Fluid Mech. **37**, 799–825 (1969).
[2]M. Li and J. G. Brasseur, "Non-steady peristaltic transport in finite-length tubes," J. Fluid Mech. **248**, 129–151 (1993).
[3]P. J. Yang, M. LaMarca, C. Kaminski, D. I. Chu, and D. L. Hu, "Hydrodynamics of defecation," Soft Matter **13**, 4960–4970 (2017).
[4]J. B. Shukla and S. P. Gupta, "Peristaltic transport of a power-law fluid with variable consistency," J. Biomech. Eng. **104**, 182–186 (1982).
[5]L. M. Srivastava and V. P. Srivastava, "Peristaltic transport of a power-law fluid: Application to the ductus efferentes of the reproductive tract," Rheol. Acta **27**, 428–433 (1988).
[6]M. K. Chaube, D. Tripathi, O. A. Bég, S. Sharma, and V. S. Pandey, "Peristaltic creeping flow of power law physiological fluids through a nonuniform channel with slip effect," Appl. Bionics Biomech. **2015**, 152802.
[7]J. C. Misra and S. K. Pandey, "A mathematical model for oesophageal swallowing of a food-bolus," Math. Comput. Modell. **33**, 997–1009 (2001).
[8]R. K. Avvari, "Effect of local longitudinal shortening on the transport of luminal contents through small intestine," Acta Mech. Sin. **35**, 45–60 (2019).
[9]T. Takahashi, "Flow behavior of digesta and the absorption of nutrients in the gastrointestine," J. Nutr. Sci. Vitaminol. **57**, 265–273 (2011).
[10]P. R. Kiela and F. K. Ghishan, "Physiology of intestinal absorption and secretion," Best Pract. Res. Clin. Gastroenterol. **30**, 145–159 (2016).
[11]R. J. A. Agbesi and N. R. Chevalier, "Flow and mixing induced by single, colinear, and colliding contractile waves in the intestine," Phys. Rev. Fluids **7**, 043101 (2022).
[12]Y. Shikaya, Y. Takase, R. Tadokoro, R. Nakamura, M. Inaba, and Y. Takahashi, "Distribution map of peristaltic waves in the chicken embryonic gut reveals importance of enteric nervous system and inter-region cross talks along the gut axis," Front. Cell Dev. Biol. **10**, 827079 (2022).
[13]T. Javed, A. H. Hamid, B. Ahmed, and N. Ali, "Effect of high Reynolds number on hydromagnetic peristaltic flow in an inclined channel using finite element method," J. Korean Phys. Soc. **71**, 950–962 (2017).
[14]T. Javed, A. H. Hamid, and N. Ali, "Numerical study of peristaltic motion of non-Newtonian fluid at high Reynolds number in an axisymmetric tube," J. Braz. Soc. Mech. Sci. Eng. **41**, 104 (2019).
[15]A. H. Hamid, T. Javed, B. Ahmed, and N. Ali, "Numerical study of two-dimensional non-Newtonian peristaltic flow for long wavelength and moderate Reynolds number," J. Braz. Soc. Mech. Sci. Eng. **39**, 4421–4430 (2017).
[16]T. Oyama, S. Ishida, K. Maeyama, T. Miyagawa, and Y. Imai, "Liquid transport produced by a cluster of peristaltic contractions in a circular channel," Phys. Rev. Fluids **6**, 093102 (2021).
[17]B. Taghilou, M. Pourjafar, and K. Sadeghy, "On the use of peristaltic waves for the transport of soft particles: A numerical study," Phys. Fluids **32**, 062108 (2020).
[18]O. Ashtari, M. Pourjafar-Chelikdani, K. Gharali, and K. Sadeghy, "Peristaltic transport of elliptic particles: A numerical study," Phys. Fluids **34**, 023314 (2022).
[19]M. Pourjafar-Chelikdani, B. Taghilou, N. P. Khabazi, A. M. Nejad, and K. Sadeghy, "On the role played by extensional viscosity in peristaltic transport of circular solid particles suspended in Oldroyd-B liquids," Phys. Fluids **34**, 073104 (2022).
[20]T. Krüger, H. Kusumaatmaja, A. Kuzmin, O. Shardt, G. Silva, and E. M. Viggen, *The Lattice Boltzmann Method* (Springer, Cham, 2017).
[21]I. Ginzburg, "A free-surface lattice Boltzmann method for modelling the filling of expanding cavities by Bingham fluids," Philos. Trans. R. Soc. A **360**, 453–466 (2002).
[22]S. Gabbanelli, G. Drazer, and J. Koplik, "Lattice Boltzmann method for non-Newtonian (power-law) fluids," Phys. Rev. E **72**, 046312 (2005).
[23]M. Yoshino, Y. Hotta, T. Hirozane, and M. Endo, "A numerical method for incompressible non-Newtonian fluid flows based on the lattice Boltzmann method," J. Non-Newtonian Fluid Mech. **147**, 69–78 (2007).
[24]C. H. Wang and J. R. Ho, "A lattice Boltzmann approach for the non-Newtonian effect in the blood flow," Comput. Math. Appl. **62**, 75–86 (2011).
[25]A. Vikhansky, "Lattice-Boltzmann method for yield-stress liquids," J. Non-Newtonian Fluid Mech. **155**, 95–100 (2008).
[26]Z. Chai, B. Shi, Z. Guo, and F. Rong, "Multiple-relaxation-time lattice Boltzmann model for generalized Newtonian fluid flows," J. Non-Newtonian Fluid Mech. **166**, 332–342 (2011).
[27]M. M. Molla, P. Nag, S. Thohura, and A. Khan, "A graphics process unit-based multiple-relaxation-time lattice Boltzmann simulation of non-Newtonian fluid flows in a backward facing step," Computation **8**, 83 (2020).
[28]S. Adam, F. Hajabdollahi, and K. N. Premnath, "Cascaded lattice Boltzmann modeling and simulations of three-dimensional non-Newtonian fluid flows," Comput. Phys. Commun. **262**, 107858 (2021).
[29]D. Conrad, A. Schneider, and M. Böhle, "Accuracy of non-Newtonian lattice Boltzmann simulations," J. Comput. Phys. **301**, 218–229 (2015).
[30]M. Geier, A. Pasquali, and M. Schönherr, "Parametrization of the cumulant lattice Boltzmann method for fourth order accurate diffusion. I. Derivation and validation," J. Comput. Phys. **348**, 862–888 (2017).
[31]R. B. Bird, W. E. Stewart, and E. N. Lightfoot, *Transport Phenomena* (John Wiley, 2002).
[32]M. Geier, M. Schönherr, A. Pasquali, and M. Krafczyk, "The cumulant lattice Boltzmann equation in three dimensions: Theory and validation," Comput. Math. Appl. **70**, 507–547 (2015).
[33]D. Yu, R. Mei, L.-S. Luo, and W. Shyy, "Viscous flow computations with the method of lattice Boltzmann equation," Prog. Aerosp. Sci. **39**, 329–367 (2003).
[34]J. Boyd, J. Buick, and S. Green, "A second-order accurate lattice Boltzmann non-Newtonian flow model," J. Phys. A: Math. Gen. **39**, 14241–14247 (2006).
[35]P. A. Cann, N. W. Read, C. Brown, N. Hobson, and C. D. Holdsworth, "Irritable bowel syndrome: Relationship of disorders in the transit of a single solid meal to symptom patterns," Gut **24**, 405–411 (1983).
[36]R. Jian, Y. Najean, and J. J. Bernier, "Measurement of intestinal progression of a meal and its residues in normal subjects and patients with functional diarrhoea by a dual isotope technique," Gut **25**, 728–731 (1984).